Check for updates

Investigating the effect of a simplified perfume accord and dilution on the formation of mixed-surfactant microemulsions†

Marzieh Mirzamani, [ID] [a] Arnab Dawn, [ID] [a] Vinod K. Aswal, [ID] [b] Ronald L. Jones,[c] Ed D. Smith[d] and Harshita Kumari [ID] *[a]

The phase analysis of a mixed surfactant system is much more complex than that for a single surfactant system. The addition of fragrance further enhances the complexity of such colloidal systems. The wide variation in structure and log P values of perfume raw materials influence its partitioning into the micellar phase. Herein, we have created a simplified perfume accord consisting of three perfume raw materials (3-PRM) and investigated its loading within a mixed-surfactant system consisting of sodium trideceth-2 sulfate/ST2S and cocamidopropyl betaine/CAPB, along with citric acid and dipropylene glycol. We performed a systematic phase diagram analysis and identified the isotropic phases and compositions of interest. Select compositions from the phase diagram were further investigated to learn how the geometry of the surfactant self-assembly and the localization of the PRMs within the surfactant self-assembly changed when water or perfume is added. A combined small-angle neutron scattering/SANS and NMR methodology was used to identify variation in colloidal domains and positioning of perfume molecules at varying dilutions/rinse off scenarios. The results obtained were utilized to better distinguish distorted micelles from true microemulsions. The systematic investigation here provides a fundamental understanding about the self-assembly, encapsulation and perfume release from a commercially relevant mixed surfactant system.

[a]*James L. Winkle College of Pharmacy, University of Cincinnati, 231 Albert Sabin Way, MSB 3109C, Cincinnati, OH 45267, USA. E-mail: kumariha@ucmail.uc.edu*

[b]*Solid State Physics Division, Bhabha Atomic Research Center, Mumbai, Maharashtra, 400085, India*

[c]*NIST Center for Neutron Research, 100 Bureau Drive, National Institute of Standards and Technology, Gaithersburg, MD, 20899, USA*

[d]*Procter & Gamble, Mason Montgomery Road, Cincinnati, OH, 45040, USA*

† Electronic supplementary information (ESI) available. See DOI: 10.1039/d1ra03458h

Introduction

Self-assembly of surfactants into a variety of nano-architectures renders them as ubiquitous molecules in varied applications, including organic reactions,[1–4] drug delivery,[5–7] and oil recovery.[8] In the field of personal care, surfactants are utilized in formulating cosmetics and rinse-off products to act as a detergent, wetting agent, emulsifier, dispersant, foaming agent, solubilizer, or some combination thereof.[9] They have an inherent property to stabilize systems/increase the shelf-life of emulsions and/or increase the penetration of actives into the skin or hair.[10] The stabilizing property is often correlated with their self-assembly in solution.

Surfactants are broadly shown to self-assemble into (a) discrete entities such as spheres, prolate ellipsoids, cylinders[11–13] or (b) continuous geometries wherein they are connected through macroscopic distances into hexagonal (1D),[14,15] lamellar (2D)[16–18] or bicontinuous/sponge phase (3D).[19–21] These three dimensional structures, also referred to as liquid crystalline structures, provide high viscosity and fluidity to surfactants. Liquid crystalline structures yield sharp lines in X-ray studies due to the inherent order/periodicity within the network. They possess an intermediate order or a long-range order which resides between that of low viscosity liquids and crystalline solids and are often identified through phase diagrams. The clear solution and cubic crystal lattice are isotropic, whereas hexagonal and lamellar phases are often cloudy and anisotropic.

X-ray and neutron scattering can provide information to deduce the packing arrangement.[22] Small-angle neutron scattering/SANS, in particular, provides information about the shape and size of colloidal domains.[23] Polarized light microscopy can also indicate anisotropy in a sample. A more intricate and less frequently utilized method is NMR spectroscopy. The quadrupole splitting in deuterium and magnitude of splitting can yield valuable information about the degree of anisotropy. A narrow singlet is observed for an isotropic phase (micellar/cubic/sponge phase) whereas a doublet is observed for an anisotropic phase (lamellar/hexagonal). The splitting is larger for a lamellar phase than a hexagonal phase. One can also

discern two- or three-phase regions through NMR by noting the types and combinations of peak splits.

The phase analyses are much more complex for a mixed-surfactant system than for a single-surfactant system. The complexity is compounded by the addition of fragrance, which is a complex mixture of varying perfume raw materials/PRMs. Surfactant mixtures, such as an anionic surfactant with a zwitterionic cosurfactant, are commonly used in personal care formulations for various reasons, such as to make the cleanser milder, increase detergency, increase the effective temperature range, achieve fabric softening properties, and increased foaming.[24–26] These mixed-surfactant systems result in the formation of micelles composed of the surfactants in the mixture as opposed to a single surfactant. The widely varying structures and lipophilicities of the PRMs in the accord influence how a molecule partitions in the micelle. When investigated individually, the most hydrophobic perfumes were found to localize within the hydrophobic core of the micelle, hydrophilic perfumes were in the aqueous phase or partially near the hydrophilic head of the micelle, and intermediately hydrophobic perfumes varied in their degree of incorporation depending on the molecular structure.[27–29]

Herein, we have created a simplified perfume accord and investigated its loading within a mixed-surfactant system through systematic phase diagram analyses. In doing so, we were able to identify the isotropic phases and compositions of interest, which we studied further to learn how the geometry of the surfactant self-assembly and the localization of the PRMs within the surfactant self-assembly changed when water or perfume is added, and to better distinguish distorted micelles from true microemulsions. We have simulated a rinse off scenario by creating phase diagrams at varying dilutions and identified variation in colloidal domains and positioning of perfume molecules through combined SANS and NMR methodology. Specifically, we have studied encapsulation and release upon dilution of a 3-PRM accord comprising of phenylethyl alcohol, dihydromercenol and hexyl cinnamic aldehyde. The 3-PRM accord is stabilized in a sodium trideceth-2 sulfate/ST2S and cocamidopropyl betaine/CAPB mixed-surfactant system, citric acid and dipropylene glycol/DPG. The systematic investigation here provides a fundamental understanding about the self-assembly, encapsulation and perfume release from a commercially relevant mixed-surfactant system.

Methods

Materials

ST2S, CAPB, citric acid, D_2O, the 3-PRM accord, and perfume grade DPG were provided by Procter & Gamble (Cincinnati, OH, USA). Millipore (Billerica, MA, USA) water was used to develop the phase diagrams. The D_2O was from Sigma-Aldrich (St. Louis, MO, USA), and was used to prepare samples for SANS studies. All materials were used as received. The composition of the PRM mixture is shown in Table 1.

Phase diagram development

Two pseudo-ternary phase diagrams were developed at two different water dilutions of 35 wt% water and at 50 wt% water. The three corners of the diagrams were total surfactant (the mixed ST2S/CAPB system), cosolvent (DPG), and perfume (3-PRM accord). The water concentration was therefore a fourth variable that was varied over separate phase diagrams.

Specifically, the samples on each phase diagram had a constant water concentration, hence the points shown on the phase diagram represent the total surfactant/perfume/cosolvent composition of the non-water fraction. This was achieved by calculating the amount of water added to the system *via* the surfactant raw materials, then adding the remaining amount of water needed to reach the required water concentration. The ratio of sodium trideceth-2 sulfate to cocamidopropyl betaine was held constant at 6.402 : 1.098. A small amount of citric acid was added as buffer to the samples to adjust the pH to approximately 6.0. All samples were prepared at room temperature (approximately 23 °C) and allowed to equilibrate for 72 hours. After the equilibration period, the phase of the sample was assessed *via* the conditions listed in Table 2.

Rheology, microscopy, X-ray diffraction, and DLS were used in our previous work to assign the phase of each sample on a phase diagram; based on that work, trends in the sample macroscopic appearance and ratio of perfume : surfactant were identified to develop simpler conditions by which phases could be assigned. It should be noted that assignments with regards to the microemulsion and micelle–microemulsion transition phases in particular are putative, due to the difficulty in differentiating micelles distorted with oil from true microemulsions.

Compositions within and along the assumed boundaries of the transition and microemulsion regions were specifically

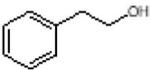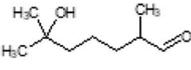**Table 1** Composition of perfume accord, with selected physical properties
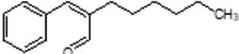
Material	Structure	Wt%	Mol. wt (g mol^{-1})	c-log P
Phenylethyl alcohol		25	122.2	1.32
Dihydromyrcenol		25	156.3	3.08
Hexyl cinnamic aldehyde		50	216.3	4.3

Table 2 Conditions for phase assignment

Phase	Conditions
Lamellar	Structured, >10 wt%/wt% surfactant, suspended air bubbles for >24 hours; similar to prior compositions determined lamellar by X-ray diffraction (not shown)
Micelle	Optically clear, isotropic, low viscosity, perfume : surfactant ratio at or below 1 : 4 wt%/wt%
Microemulsion	Optically clear, isotropic, low viscosity, perfume : surfactant ratio at or above 1 : 2 wt%/wt% (exceeding oil solubilization capacity of micelles)
Micelle–microemulsion transition	Optically clear, isotropic, low viscosity, perfume : surfactant ratio above 1 : 4 and below 1 : 2 wt%/wt%
O/W emulsion	Opaque to milky white, often separated into layers
Two-phase	Lamellar, oily, or emulsion phase present with micelle or microemulsion phase, visible separation

chosen to study any changes that occurred at these points. The compositions of each sample studied with SANS and NMR are shown in Tables 3 and 4 (35 wt% and 50 wt% water, respectively).

SANS studies

Select compositions were identified from the phase diagrams for SANS studies. The regions we believed to be micellar and microemulsion were identified as a function of perfume concentration. For select compositions, the ratio of surfactant to DPG was maintained at 1 : 1 so the concentrations of surfactant and DPG decreased at the same rate as the perfume concentration increased. This was done to minimize the effect of the decreasing surfactant and DPG concentrations, as the effect of perfume at a given water concentration was of more interest. Compositions that did not phase-separate upon dilution were also studied with SANS.

The samples containing 35 wt% water were first made by weighing surfactant, DPG, D_2O, and perfume accord into vials. A portion of the 35 wt% water samples was weighed into separate vials and then diluted to 50 wt% water with D_2O. The solvent phase of each sample therefore contained a mix of H_2O and D_2O due to the surfactants carrying H_2O. Each sample was vortexed until mixed and then set aside to equilibrate for at least 24 h. Equilibrated samples were injected into pre-assembled titanium sample holders with a 1 mm path length and quartz windows. The sample holders were then sealed to minimize evaporation.

The SANS study was conducted on the 10 m NGB-SANS beamline at the NCNR (Gaithersburg, MD, USA), operated as part of the nSoft Consortium. Three instrument configurations were used as follows: the high-q configuration consisted of 1.2 m sample-to-detector distance (SDD), a neutron wavelength of $\lambda = 5$ Å, with measurements lasting 7.5 min; the mid-q configuration had a SDD of 5.2 m, a neutron wavelength of $\lambda = 10$ Å, and a measurement time of 25 min; and the low-q configuration had a SDD of 5.2 m, a beam wavelength of $\lambda = 10$ Å, and measurement time of 50 min. Reduction macros for Igor Pro provided by NIST were used to reduce the raw data to correct for background scattering, detector sensitivity and resolution, instrument geometry, and beam transmission. The reduced data were set to absolute scale by radial averaging, and then combined to create the complete data set spanning a q-range of 0.006 Å^{-1} <q< 0.53 Å^{-1}. All measurements were performed at approximately 22 °C.

NMR studies

^{1}H-NMR was run in a Bruker AV 400 MHz spectrometer (Billerica, MA, USA). Samples were made 3 days before running on NMR. The solvent was a mix of H_2O and D_2O, as H_2O was added to the system *via* the surfactants and D_2O was added separately to reach the required water concentration. The H_2O peak at 4.69 ppm was used as the reference for data analysis.

Results and discussion

Pseudo-ternary phase diagrams

Phase diagrams were primarily developed to learn what combinations of surfactant, DPG, and 3-PRM accord create microemulsions at each dilution level, and how the region

Table 3 Compositions, in wt%, of SANS and NMR samples containing a total of 35 wt% water

Code	Wt% component						
	ST2S	CAPB	DPG	perfume	Citric Acid	H$_2$O	D$_2$O
L1-noPRM-35	27.74	4.76	32.50	0.00	0.48	26.04	8.48
L1-35	26.35	4.52	30.88	3.25	0.45	24.74	9.81
L1T-35	24.66	4.23	28.89	7.22	0.42	23.14	11.44
T-35	23.36	4.01	27.37	10.26	0.40	21.93	12.67
MeT-35	22.19	3.81	26.00	13.00	0.38	20.83	13.79
Me-35	20.81	3.57	24.38	16.25	0.36	19.53	15.11
MeB-35	18.86	3.24	22.10	20.80	0.32	17.02	17.66

Table 4 Compositions, in wt%, of SANS and NMR samples containing a total of 50 wt% water

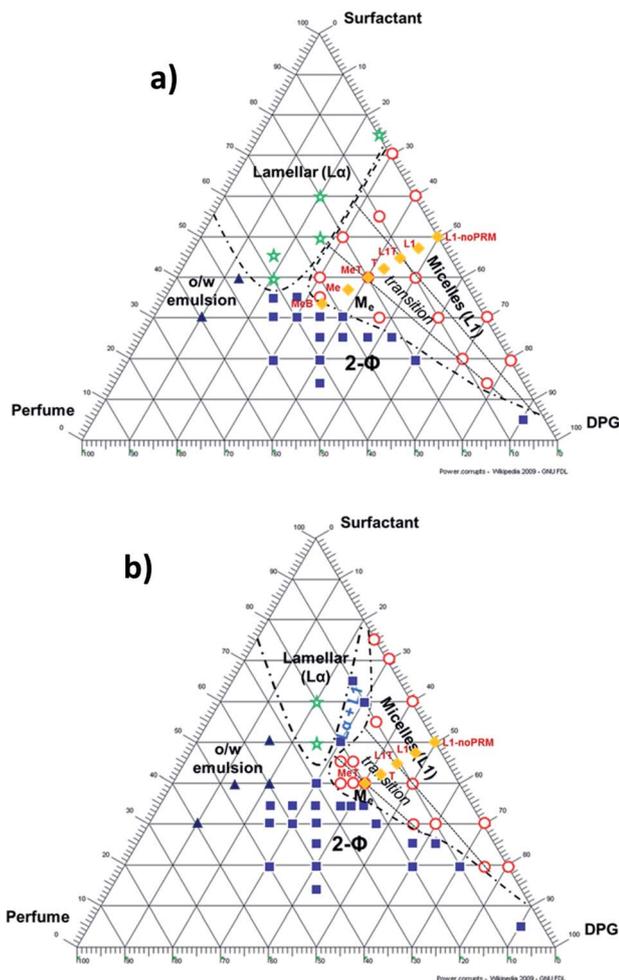| Code	Wt% component						
	ST2S	CAPB	DPG	Perfume	Citric acid	H$_2$O	D$_2$O
L1-noPRM-50	21.34	3.66	25.00	0.00	0.37	20.03	29.60
L1-50	20.27	3.48	23.75	2.50	0.35	19.03	30.62
L1T-50	18.97	3.25	22.22	5.56	0.33	17.80	31.88
T-50	17.97	3.08	21.05	7.89	0.31	16.87	32.82
MeT-50	17.07	2.93	20.00	10.00	0.29	16.02	33.68
Me-50	16.01	2.75	18.75	12.50	0.28	15.02	34.70
MeB-50	14.51	2.49	17.00	16.00	0.25	13.09	36.66

Fig. 1 Pseudo-ternary phase diagrams of 3-PRM perfume accord, sodium trideceth-2 sulfate/cocamidopropyl betaine (ST2S/CAPB) mixed-surfactant system, dipropylene glycol (DPG), and water: (a) 35 wt% water, (b) 50 wt% water. Circles (○) denote transparent compositions, filled squares (■) are compositions that separated into multiple distinct phases, triangles (▲) are compositions that were milky white emulsions, stars (☆) show compositions that were viscous and held bubbles for long periods of time, and diamonds (◆) are the compositions tested with SANS.

boundaries shift with dilution. Once this information was determined, the diagrams were used to plan other experiments. Fig. 1 shows the phase diagrams that were developed at (a) 35 wt% water and (b) 50 wt% water. Many compositions were tested to thoroughly define the micelle (L1) and microemulsion (Me) regions. The compositions falling in other regions, such as lamellar (Lα) and two-phase (2-Φ) regions, were noted but the regions were not fully explored as the microemulsion region was of greater interest. A so-called "transition" (T) region was marked between the L1 and Me regions to note where micelles and microemulsion structures would theoretically coexist, assuming that they are two distinct phases. The L1T border comprises of compositions containing a perfume : surfactant ratio of 1 : 4, whereas the Me–T border is compositions containing a perfume : surfactant ratio of 1 : 2. Of the three

optically clear, isotropic regions (i.e. L1, T, and Me), the Me region was of the greatest interest due to its high oil-loading capability. Phase diagrams were developed at increasing water concentrations until the Me region almost disappeared.

Fig. 1a shows that the L1, T, and Me regions are approximately the same size. They do not make up a large portion of the diagram altogether, and appear approximately similar in size to the Lα region. Once diluted to 50 wt% water (Fig. 1b), the Me region dramatically shrank to nearly disappearing, while the T region shrank to about half its original size. The L1 region expanded slightly toward the surfactant corner and retracted somewhat from the DPG corner, thus remaining approximately the same size overall. The Me region's strong reaction to added water suggests that this combination of surfactant, cosolvent, and perfume accord does not support the formation of MEs very well. Instead of maintaining the ME structure at higher water concentrations, the system phase-separates.

Samples containing 35 wt% water

Two models were required to model the SANS data for the samples containing 35 wt% water. The first model was a resolution-smeared sphere form factor and hard sphere structure factor with monodisperse approximation model, which was used for the micelles with no perfume sample (L1-noPRM), micelles with perfume sample (L1), the sample on the border of the micelle-transition region (L1T), and the sample in the transition region (T). The sample bordering the microemulsion-transition region (MeT), the microemulsion sample (Me), and the sample on the outside border of the microemulsion region (MeB) were modeled with a resolution-smeared ellipsoid model combined with the equivalent hard sphere structure factor with beta decoupling approximation. An overlay of the scattering data and their model fits is shown in Fig. 2. The switch in models as the perfume concentration increased suggested
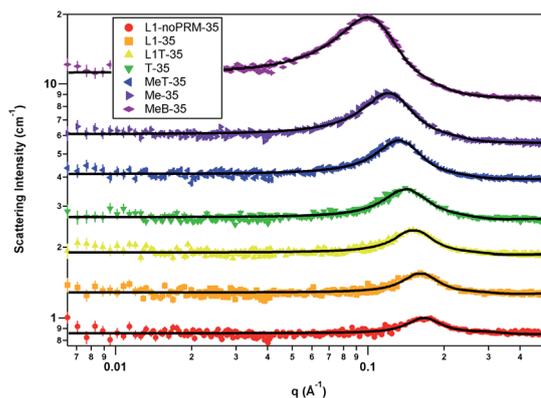

Fig. 2 SANS data overlay of all samples containing 35 wt% water. L1-noPRM-35, L1-35, L1T-35, and T-35 were fitted with a sphere form factor and hard sphere structure factor model with monodisperse approximation. MeT-35, Me-35, and MeB-35 were fitted with a uniform ellipsoid form factor and hard sphere structure factor model with decoupling approximation. Each data set except for L1-noPRM-35 was offset by powers of 1.5 to better distinguish them. The solid black lines are the model fits to the scattering data.

Table 5 SANS fitting results for the samples containing 35 wt% water. The L1-noPRM, L1, L1T, and T samples were fitted with the sphere form factor and hard sphere structure factor with monodisperse approximation, while the MeT, Me, and MeB samples were fitted with the ellipsoid form factor and MSA structure factor with decoupling approximation

Parameter	L1-noPRM-35	L1-35	L1T-35	T-35	MeT-35	Me-35	MeB-35
Volume fraction	0.38	0.37	0.35	0.34	0.32	0.29	0.25
R_a rotation axis (Å)	9.77	11.37	12.01	12.29	9.34	9.62	10.35
R_b (Å)	9.77	11.37	12.01	12.29	16.28	17.50	22.01
Effective radius (Å)	19.40	19.79	20.73	22.03	22.94	24.90	28.58
Volume (Å^3)	3911	6157	7258	7772	10 373	12 336	20 987
Aspect ratio	1.00	1.00	1.00	1.00	1.74	1.82	2.13

a change in the *d*-spacing of the self-assembly. The mean spherical approximation structure factor of interacting charged spheres was also tested for all samples, as significant electrostatic repulsions were expected in these systems due to the use of anionic surfactants. However, the fitted charge values were low while the effective radii from the structure factor calculations were relatively large, suggesting that the systems were primarily sterically stabilized rather than charge stabilized. Using the hard sphere structure factor instead resulted in better quality fits with fewer required parameters.

As perfume content increased from the L1-noPRM through T samples, the volume fraction consistently decreased as perfume was titrated into the system. Additionally, the radius and volume of the scattering particles increase as perfume is added, indicating that the added perfume is taken up in the surfactant assembly (Table 5). These trends suggest that the volume fraction decreased because the surfactant concentration decreased to account for the increasing perfume concentration, resulting in fewer but larger globules that made up a smaller portion of the overall system. Past the transition region, a change to the geometry of the assembly in the MeT, Me, and MeB samples occurs (Table 5). The assembly became ellipsoidal instead of spherical possibly due to the large amount of perfume loaded into the assembly relative to the amount of surfactant in the system. Due to how the ellipsoid model functions, if $R_a > R_b$ then the micelle is a prolate ellipsoid, and if $R_a < R_b$ then the micelle is an oblate ellipsoid. Therefore, the micelles in these three samples formed oblate ellipsoids. As perfume was added, R_a gradually lengthened from 9.32 Å to 10.35 Å in samples MeT

and MeB respectively. R_b was more strongly affected by the perfume addition, especially seen by the 5 Å increase from sample Me to MeB. The increasing micelle volume again indicates that the perfume was solubilized into the micelles. The increasing micelle volume and decreasing volume fraction values continue following the trends of the L1-noPRM, L1, L1T, and T samples. The effective radius is the radius within which no other particle can enter; in other words, the particles are hard spheres. The effective radius is consistently larger than R_a and R_b because the R_a and R_b are primarily the dimensions of the oil core of the micelles, so the effective radius includes the shell in addition to the core. This is because the micelle shell cannot be distinguished from the solvent in SANS data due to their similar compositions and solvation of the surfactant headgroups. The effective radius also increased with R_a and R_b (but at a separate rate) as the perfume concentration increased, further demonstrating that the perfume was incorporated into the core of the structure.

^{1}H-NMR studies were conducted on L1-noPRM through MeB in a mixture of H_2O and D_2O in order to assess the localization sites of various components. The individual components—namely ST2S, CAPB, DPG, citric acid, and the 3-PRM mixture (solubilized with a small amount of the mixed-surfactant system)—were first dissolved in D_2O. Spectra of the individual components were obtained to identify and assign the peaks associated with each component. Spectra for the seven samples, L1-noPRM through MeB, were then obtained, and the peaks corresponding to each component were assigned and followed under varying system compositions. To analyse the effect of

Table 6 Differential chemical shifts[a] of ST2S signals (1, 2, 3, 4) with respect to L1-noPRM, and signal corresponding to three perfume mixture (a–l) with respect to L1, in the systems containing 35 wt% H_2O/D_2O mixture

Sample	1	2	3	4	a	b	c	d	e	f	h	i	j	l
L1-noPRM-35	0.00	0.00	0.00	0.00	—	—	—	—	—	—	—	—	—	—
L1-35	−0.02	−0.02	0.00	0.00	0.00	0.00	0.00	0.00	0.00	0.00	0.00	0.00	0.00	0.00
L1T-35	−0.05	−0.05	−0.01	0.00	−0.05	−0.04	−0.05	−0.04	−0.02	−0.01	−0.04	−0.04	−0.03	−0.03
T-35	−0.08	−0.07	−0.01	−0.01	−0.08	−0.08	−0.09	−0.08	−0.04	−0.03	−0.07	−0.08	−0.06	−0.05
MeT-35	−0.10	−0.10	−0.02	−0.02	−0.11	−0.10	−0.11	−0.10	−0.05	−0.03	−0.09	−0.11	−0.07	−0.07
Me-35	−0.14	−0.12	−0.03	−0.03	−0.14	−0.14	−0.15	−0.14	−0.07	−0.06	−0.12	−0.15	−0.09	−0.10
MeB-35	−0.16	−0.14	−0.03	−0.03	−0.17	−0.17	−0.19	−0.20	−0.08	−0.08	−0.14	−0.19	−0.11	−0.11

[a] Negative sign signifies upfield shift or shielding.
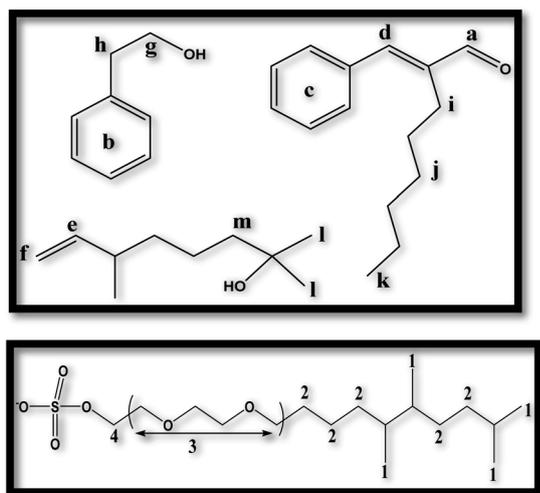
Scheme 1 Molecular structures and proton signal labels for: (top) the three PRMs, (bottom) ST2S. The PRMs are, listed clockwise from top left, phenylethyl alcohol, hexylcinnamic aldehyde, and dihydromyrcenol.

perfume on the ST2S/CAPB micellar assembly, the L1-noPRM sample was used as the reference to calculate differential changes in NMR signals associated with ST2S due to the addition of perfume in the sample. Likewise, the L1 sample with lowest amount of perfume was used as the reference for further analysing the changes in perfume molecules in relation to the interaction with ST2S, because L1 contained the lowest concentration of perfume.

As seen in Table 6 and Fig. S1 (see ESI†), the proton signals (1 and 2) (Scheme 1) associated with the hydrophobic tail group of ST2S shifted upfield as perfume was added, indicating increased shielding. In contrast, the proton signals (3 and 4) related to the polar head group region of ST2S shifted upfield to a much lesser extent with the addition of perfume (refer to Scheme 1 for proton assignments). These results show that the perfume molecules preferentially interacted with the hydrophobic tail group of ST2S, and are therefore localized near the core of the micellar assembly regardless of chemical nature of each perfume molecule. Additionally, hexyl cinnamic aldehyde and phenylethyl alcohol, the PRMs with the highest and lowest log P values at 4.3 and 1.3, respectively, exhibited stronger interactions with ST2S (greater extent of upfield shift) than dihydromyrcenol, which had an intermediate log P value of 3.1. Therefore, the lipophilicity or hydrophilicity of the individual PRMs no longer become important; instead, the complete perfume accord acts as a single entity when interacting with the surfactant. As such effect becomes most prominent in presence of highest content of perfume accord, intermolecular interactions among the perfume molecules (especially at enhanced concentration) might be a contributing factor for this. Lastly, it was observed from the consistent changes in NMR signal that the mixed-surfactant assembly underwent a continuous transformation from micelle (L1) to microemulsion (Me) *via* a transition region (T).

Table 7 SANS fitting results for the samples containing 50 wt% water, using the ellipsoid model with the hard sphere structure factor

Parameter	L1-noPRM-50	L1-50	L1T-50	T-50	MeT-50
Volume fraction	0.34	0.33	0.31	0.30	0.29
R_a rotation axis (Å)	10.96	11.11	12.07	12.37	13.06
R_b (Å)	17.34	18.82	20.50	22.77	25.25
Effective radius (Å)	22.86	24.03	25.92	28.27	30.72
Volume (Å^3)	13 805	16 475	21 230	26 851	34 851
Aspect ratio	1.58	1.69	1.70	1.84	1.93

Samples containing 50 wt% water

Only the ellipsoid model with the hard sphere structure factor with decoupling approximation was needed to model all five samples containing 50 wt% water, namely the L1-noPRM, L1, L1T, T, and MeT samples. Table 7 shows the SANS fitting results while Fig. 3 shows the scattering data overlay complete with model fits to the data. The assemblies in all five samples maintained the oblate ellipsoid geometry, and the structures grew in size as the perfume concentration increased. The volume fraction consistently decreased as the perfume concentration increased, R_a steadily increased from 10.96 Å to 13.06 Å with added perfume, and R_b was more strongly influenced by the perfume concentration, such that it increased from 17.34 Å to 25.25 Å. As a result, the micelle volume increased from 13 804.76 Å^3 to 34 851.08 Å^3 as the perfume content increased, indicating that the additional perfume was incorporated into the assembly. As previously noted, the volume fraction likely decreased due to fewer globules forming as the surfactant concentration decreased while perfume was added. In addition, the effective radius was again larger than R_a and R_b because it includes the surfactant headgroups, whereas R_a and R_b are the dimensions of the micelle core only. The effective radius grows with R_a and R_b as perfume is added, as would be expected.
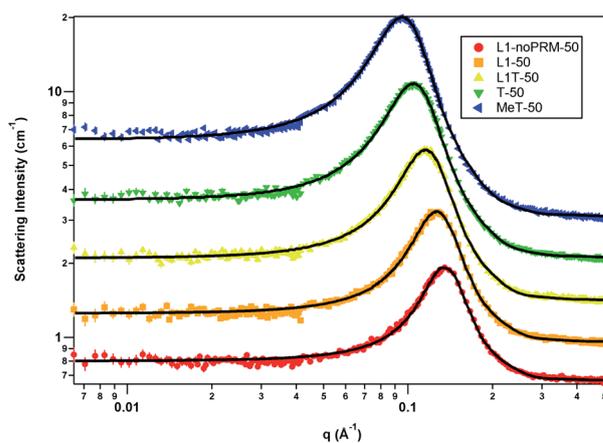

Fig. 3 SANS data overlay of all samples containing 50 wt% water. They were fitted with a uniform ellipsoid form factor and hard sphere structure factor model with beta approximation. Each data set except for L1-noPRM-50 was offset by powers of 1.5 to better distinguish them. The solid black lines are the model fits to the scattering data.

Table 8 Differential chemical shifts[a] of ST2S signals (1, 2, 3, 4) with respect to L1–noPRM, and signal corresponding to three perfume mixture (a–l) with respect to L1, in the systems containing 50 wt% H_2O/D_2O mixture. Scheme 1 shows the molecular structures and proton signal labels for the three PRMs and ST2S

Sample	1	2	3	4	a	b	c	d	e	f	h	i	j	l
L1-noPRM-50	0.00	0.00	0.00	0.00	—	—	—	—	—	—	—	—	—	—
L1-50	−0.03	−0.04	0.02	−0.01	0.00	0.00	0.00	0.00	0.00	0.00	0.00	0.00	0.00	0.00
L1T-50	−0.07	−0.08	−0.03	−0.02	−0.05	−0.06	−0.05	−0.1	−0.03	−0.02	−0.05	−0.05	−0.04	−0.03
T-50	−0.09	−0.11	−0.03	−0.02	−0.10	−0.11	−0.09	−0.16	−0.04	−0.03	−0.08	−0.09	−0.06	−0.06
MeT-50	−0.10	−0.11	−0.04	−0.03	−0.13	−0.15	−0.12	−0.22	−0.06	−0.04	−0.11	−0.13	−0.08	−0.08
Me-50	−0.12	−0.11	−0.04	−0.04	−0.16	−0.17	−0.16	−0.28	−0.07	−0.05	−0.14	−0.17	−0.10	−0.10
MeB-50	−0.13	−0.12	−0.05	−0.04	−0.18	−0.19	−0.18	−0.30	−0.08	−0.06	−0.15	−0.19	−0.11	−0.11

[a] Negative sign signifies upfield shift or shielding.

^{1}H-NMR data of the samples containing 50 wt% H_2O/D_2O did not reflect any significant differences caused by dilution (Table 8 and Fig. S2,-see ESI†). The perfume molecules still preferentially interacted with the surfactant hydrophobic region and therefore remained near the micelle core. However, two new changes could be identified with the increase in dilution: first, there was a somewhat greater extent of interaction with the hydrophilic head group region of ST2S; and second, the perfume–surfactant interaction became stronger. The larger mixed-surfactant assemblies may have allowed the perfume molecules to become more distributed, causing the intermolecular interactions between them to be reduced. As a result, the perfume–surfactant interaction was strengthened (associated with greater shielding of the perfume molecules), and the perfume molecules became somewhat less localized (related to increased shielding of the surfactant head groups).

Effect of dilution and micelles *vs.* microemulsions

Interesting trends were identified when comparing how the size and geometry of each composition changed as a function of water concentration. MeT at both dilutions was fitted with the same model allowing a direct comparison in the geometry and size of the particles. When the water concentration increased from 35 wt% to 50 wt%, the oblate ellipsoid geometry of MeT remained constant but the overall volume increased thrice due to an increase in the length of both R_a and R_b from 9.34 Å to 13.06 Å for 35 wt% and from 16.28 Å to 25.25 Å for 50 wt%. Interestingly, the sizes of the structures in the L1–noPRM and L1 samples at 50 wt% water were somewhat larger than the sizes of the particles in the Me sample at 35 wt% water, suggesting that the particle volumes grew as the compositions were diluted. These overall effects show that with increased dilution, oblate ellipsoids are a more thermodynamically favourable geometry. It appears that there are local compositional differences that drive the change in curvature across the structure, but it is unclear what kind of interactions are compensating for the entropic loss related to those local compositional differences. Finally, diluting the Me and MeB samples from 35 wt% to 50 wt% caused both compositions to phase-separate as there was not enough surfactant to stabilize the interface between the oil and water phases.

This data also permits us to comment on the differences between micellar structures and microemulsion structures. It is known that a typical sodium dodecylsulfate (SDS) micelle is approximately 35–37 Å in diameter,[30,31] which would be 22 450–26 522 Å^3. All the samples containing 35 wt% water consist of micelles smaller in volume than a SDS micelle, as shown in Fig. 4a. The smallest dimension of these micelles, R_a, becomes longer than the length of the extended tail group, 11.32 Å (see ESI†), as soon as perfume is added at 5 wt% (actives basis), suggesting that these micelles begin to swell once perfume is added. The micelles continue to swell to 8.6% with the addition of 15 wt% (actives basis, corresponding to sample T) perfume in the 35 wt% water samples. Upon further perfume addition, the aspect ratio of these structures changes from 1 (spherical) to 1.7 (oblate ellipsoidal, Fig. 4b) and R_a becomes smaller than the extended length of the tail group; thus, the micelles are distorted but no longer swollen. Additionally, the aspect ratio continues to increase when more perfume was added, suggesting that the perfume preferentially packs along the longer axis (R_b) to create flatter micelles. Once water is added to reach a total water content of 50 wt%, the point at which the micelles finally become larger than SDS micelles is when the perfume content is close to 11 wt% (actives basis). R_a becomes longer than the extended length of the tail group at 10 wt% perfume (corresponding to L1T) at 50 wt% water concentration, indicating that swelling can begin at somewhat lower perfume concentrations if the water concentration is high enough. These trends suggest that micelles and microemulsions can be
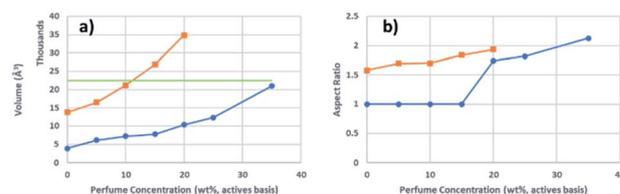

Fig. 4 (a) Self-assembly volume *vs.* perfume concentration (actives basis, disregarding the water portion) and (b) aspect ratio *vs.* perfume concentration (actives basis, disregarding the water portion). Blue circles are the samples containing 35 wt%, orange squares are the samples containing 50 wt% water, and green line denotes the volume of typical SDS micelles.

differentiated by the volume of the aggregates and when the smaller dimension becomes larger than the extended length of the surfactant tail group. These trends also indicate that although increasing the perfume : surfactant ratio can distort the micelle from swollen spheres to ellipsoids, the water concentration must be high enough to allow a complete phase change from micelles to a microemulsion. Finally, it appears that the assumed perfume : surfactant ratios that mark the boundaries of the transition region, outlined in Table 2, are approximately accurate.

Conclusions

Pseudo-ternary phase diagrams demonstrate that the combination of sodium trideceth-2 sulfate as primary surfactant, cocamidopropyl betaine as cosurfactant, dipropylene glycol, and a perfume accord consisting of phenylethyl alcohol, dihydromyrcenol, and hexylcinnamic aldehyde is not very capable of forming MEs, or of maintaining MEs under increasing dilution. SANS fitting results showed that the self-assemblies at 35 wt% water consistently grew as a function of perfume addition, and that a change in geometry from spheres to oblate ellipsoids could be induced when a sufficient amount of perfume was added to the system. Additionally, diluting the system to 50 wt% water resulted in the self-assembly becoming even larger. Further interpretation of the SANS trends also indicated that micelles and microemulsions could be differentiated by the volume and degree of swelling of the aggregates, and that enough water must be present in the system to allow for the complete transition from the micelle phase to the microemulsion phase. ^{1}H-NMR determined that the 3 PRMs were preferentially localized in the core of the micelles despite their respective lipophilicities at 35 wt% water, suggesting that intermolecular interactions between the PRMs had a strong influence on their location. Although diluting the systems did not cause a significant relocation of the PRMs in the assembly or a rearrangement of the system, the larger assembly volume with dilution reduced the intermolecular interactions between the PRMs, thereby allowing them to redistribute somewhat within the assembly based on the perfume–surfactant interaction. Additionally, the lack of any break in the shift of the peak as perfume was added suggests that the transition from micelles to MEs is continuous. These findings suggest that finding beneficial interactions between the PRMs of interest, utilizing a surfactant system that forms self-assemblies of a structure that is conducive to perfume release, and choosing a suitable perfume : surfactant ratio are methods that can be explored to better incorporate perfumes in rinse-off formulations.

Author contributions

MM: wrote the main manuscript text, revised/reviewed manuscript for final version approval, prepared figures, concept, design, and partial literature review for the research, and carried out experimental studies at NIST. AD: performed, analysed and wrote NMR experimental section. VA: helped with SANS data analyses. RJ: helped with SANS instrument settings for data measurement. ES: guided for experimental design and analyses. HK: supervised the whole project and guided for all the experiments, including writing, editing, revision/reviewing of manuscript.

Conflicts of interest

There are no conflicts to declare.

Acknowledgements

Notes and references

1 K. Holmberg, *Curr. Opin. Colloid Interface Sci.*, 2003, **8**, 187–196.

2 N. L. Klyachko and A. V. Levashov, *Curr. Opin. Colloid Interface Sci.*, 2003, **8**, 179–186.

3 M. A. Malik, M. Y. Wani and M. A. Hashim, *Arabian J. Chem.*, 2012, **5**, 397–417.

4 T. Wielputz, T. Sottmann, R. Strey, F. Schmidt and A. Berkessel, *Chemistry*, 2006, **12**, 7565–7575.

5 M. Fanun, *Curr. Opin. Colloid Interface Sci.*, 2012, **17**, 306–313.

6 M. J. Lawrence and G. D. Rees, *Adv. Drug Delivery Rev.*, 2000, **45**, 89–121.

7 S. P. Callender, J. A. Mathews, K. Kobernyk and S. D. Wettig, *Int. J. Pharm.*, 2017, **526**, 425–442.

8 J. L. Salager, A. M. Forgiarini, L. Marquez, L. Manchego and J. Bullon, *J. Surfactants Deterg.*, 2013, **16**, 631–663.

9 M. M. Rieger, Surfactant chemistry and classification, in *Surfactants in Cosmetics, Surfactant Science Series*, ed. M. M. Rieger and L. D. Rhein, Marcel Dekker, New York, 2nd edn, 1997.

10 Y. Nakama, Surfactants, in *Cosmetic Science and Technology: Theoretical Principles and Applications*, ed. K. Sakamoto, R. Y. Lochhead, H. I. Maibach and Y. Yamashita, Elsevier, Amsterdam, Netherlands, 2017.

11 G. Verma, V. K. Aswal, G. Fritz-Popovski, C. P. Shah, M. Kumar and P. A. Hassan, *J. Colloid Interface Sci.*, 2011, **359**, 163–170.

12 C. Ade-Browne, A. Dawn, M. Mirzamani, S. Qian and H. Kumari, Differential behavior of sodium laurylsulfate micelles in the presence of nonionic polymers, *J. Colloid Interface Sci.*, 2019, **544**, 276–283.

13 S. He, N. Joseph, M. Mirzamani, S. J. Pye, A. H. M. Al-Anataki, A. E. Whitten, Y. Chen, H. Kumari and C. L. Raston, *NPJ Sci. Food*, 2020, **4**, 12.

14 M. M. Alam, Y. Matsumoto and K. Aramaki, *J. Surfactants Deterg.*, 2013, **17**, 19–25.

15 D. Jurašin, M. Vinceković, A. Pustak, I. Šmit and M. Bujan, *Soft Matter*, 2013, **9**, 3349–3360.

16 M. Bergstrom, J. Pedersen, P. Schurtenberger and S. Egelhaaf, *J. Phys. Chem. B*, 1999, **103**, 9888–9897.

17 Y. Suganuma, N. Urakami, R. Mawatari, S. Komura, K. Nakaya-Yaegashi and M. Imai, *J. Chem. Phys.*, 2008, **129**(13), 134903.

18 C. Ade-Browne, M. Mirzamani, A. Dawn, S. Qian, R. G. Thompson, R. W. Glenn and H. Kumari, *Colloids Surf., A*, 2020, **595**, 124704.

19 D. G. Hayes, R. Ye, R. N. Dunlap, D. B. Anunciado, S. V. Pingali, H. M. O'Neill and V. S. Urban, *Biochim. Biophys. Acta, Biomembr.*, 2018, **1860**, 624–632.

20 D. G. Hayes, R. Ye, R. N. Dunlap, M. J. Cuneo, S. V. Pingali, H. M. O'Neill and V. S. Urban, *Colloids Surf., B*, 2017, **160**, 144–153.

21 M. Laupheimer, T. Sottmann, R. Schweins and C. Stubenrauch, Studying orthogonal self-assembled systems: microstructure of gelled bicontinuous microemulsions, *Soft Matter*, 2014, **10**, 8744–8757.

22 (*a*) R. S. Patil, A. M. Drachik, H. Kumari, C. L. Barnes, C. A. Deakyne and J. L. Atwood, *Cryst. Growth Des.*, 2015, **15**(6), 2781–2786; (*b*) R. S. Patil, H. Kumari, C. L. Barnes and J. L. Atwood, *Chem.–Eur. J.*, 2015, **21**(29), 10431–10435; (*c*) R. S. Patil, H. Kumari, C. L. Barnes and J. L. Atwood, *Chem. Commun.*, 2015, **51**(12), 2304–2307; (*d*) H. Kumari, S. R. Kline, S. R. Kennedy, C. Garvey, C. L. Raston, J. L. Atwood and J. W. Steed, *Chem. Commun.*, 2016, **52**,

4513–4516; (*e*) H. Kumari, S. E. Armitage, S. R. Kline, K. K. Damodaran, S. R. Kennedy, J. L. Atwood and J. W. Steed, *Soft Matter*, 2015, **11**(43), 8471–8478.

23 (*a*) H. Kumari, W. Wycoff, C. Mayhan, S. R. Kline, J. So, C. A. Deakyne, J. E. Adams and J. L. Atwood, *RSC Adv.*, 2021, **11**, 3342–3345; (*b*) H. Kumari, C. A. Deakyne and J. L. Atwood, *Acc. Chem. Res.*, 2014, **47**(10), 3080–3088.

24 P. M. Holland and D. N. Rubingh, Mixed surfactant systems, in *Mixed Surfactant Systems*, ACS Symposium Series, 1992, pp. 2–30.

25 D. Myers, Physical properties of surfactants used in cosmetics, in *Surfactants in Cosmetics, Surfactant Science*, ed. M. Rieger and L. D. Rhein, CRC Press, 2nd edn, 1997, pp. 29–82.

26 T. Sakai, Body Care Cosmetics, in *Cosmetic Science and Technology: Theoretical Principles and Applications*, ed. K. Sakamoto, R. Y. Lochhead, H. I. Maibach and Y. Yamashita, Elsevier, 2017, pp. 561–570.

27 E. Fischer, W. Fieber, C. Navarro, H. Sommer, D. Benczédi, M. I. Velazco and M. Schönhoff, *J. Surfactants Deterg.*, 2009, **12**, 73–84.

28 Y. Fan, H. Tang, R. Strand and Y. Wang, *Soft Matter*, 2016, **12**, 219–227.

29 V. V. Suratkar and S. Mahapatra, *J. Colloid Interface Sci.*, 2000, **225**, 32–38.

30 G. Duplâtre, M. F. Ferreira Marques and M. Da Graça Miguel, *J. Phys. Chem.*, 1996, **100**, 16608–16612.

31 T. E. Burchfield and E. M. Woolley, *J. Phys. Chem.*, 1984, **88**, 2149–2155.